Structures 82 (2025) 110648

Contents lists available at ScienceDirect

Structures

journal homepage: www.elsevier.com/locate/structures

A practical method to incorporate scour hole shape effects in Winkler-type pile foundation models for bridges

M. Kosič [a], L.J. Prendergast [b,*], A. Anžlin [a]

[a] Section for Bridges and Other Civil Engineering Structures, Department for Structures, Slovenian National Building and Civil Engineering Institute (ZAG), Dimičeva ulica 12, Ljubljana, Slovenia
[b] Department of Civil Engineering, Faculty of Engineering, University of Nottingham, Nottingham NG7 2RD, United Kingdom

ARTICLE INFO

Keywords:
Scour
Dynamics
Overburden
Frequency
Damage
Bridges
Scour hole shape

ABSTRACT

Scour erosion continues to cause significant issues for the stability and lifespan of bridges worldwide. In Slovenia, extreme flooding in 2023 caused the collapse or failure of many bridges, primarily due to scour, which was exacerbated by debris accumulation. Despite advances in predicting and monitoring scour, it remains among the top reasons for the failure of bridges during flooding. Recent advances in vibration-based health monitoring suggest that scour erosion can be detected using methods such as changes in natural frequency, mode shapes, flexibility-based deflection, and other approaches using offline sensors such as passing vehicle responses. Many of these methods have been trialled numerically where scour is implemented as a reduction in the soil level (or stiffness) around a given bridge foundation. The most common way to model scour is to lower the soil level around a foundation, however, this ignores any contribution that the scour hole shape makes to the stiffness and strength of the soil beneath the scour hole. This paper investigates how the shape of scour holes influences the stiffness and strength of the remaining soil to understand the impact on the modal behaviour of a bridge. A numerical model of a bridge is developed where scour is implemented by removing Winkler springs from the model, and different scour hole shapes are considered in terms of how the remaining overburden influences the stiffness and strength of the soil springs. Scour hole shape properties are considered by means of varying the depth, width, and slope angle of the hole around a given foundation element. For the analyses in this paper, different scour hole shapes are implemented on an example bridge corresponding to local scour holes with narrow width; wider local scour holes; and general scour, where the full soil layer is removed (infinite width). The changes in the modal periods and mode shapes of the bridge in the traffic and river flow directions are assessed to understand the impact of the different scour types on the vibration characteristics.

1. Introduction

Climate change, specifically the increase in global average temperature, is potentially causing more frequent and larger magnitude flooding events in certain regions worldwide [1]. Bridges are a critical part of our transport infrastructure, and are particularly vulnerable to climate change and flooding. Scour erosion, where flowing water washes away soil [2,3], affects bridges with submerged foundations. There are three main types of scour: general scour, which refers to natural changes in riverbed morphology due to changes in governing hydraulic parameters [4,5]; contraction scour, which is caused by the presence of bridge openings increasing flow velocity and corresponding bed shear stresses as the river channel width is constricted at the location of bridge substructural elements (piers and abutments) [2]; and local scour, which is caused by the presence of obstacles to the flow such as bridge piers and foundations, resulting in vortex generation [6] and downward flow that erodes the soil. Local scour can be further complicated for bridges located in coastal areas, such as sea-crossing bridges, where sediment beds might be inclined, resulting in slope-induced vortex enhancement and deeper scour holes [7]. All three forms of scour can occur at a given bridge location, and the resulting scour hole depth is the summation of these mechanisms.

Local scour poses a specific risk to bridge structures with foundations in water. The depth and width of a local scour hole that can form is a function of the water flow characteristics (flow rate, water height), the shape of the bridge elements, and the properties of the sediment. Scour can occur under relatively moderate flow conditions [8], but is

* Corresponding author.
E-mail address: luke.prendergast@nottingham.ac.uk (L.J. Prendergast).

https://doi.org/10.1016/j.istruc.2025.110648
Received 20 December 2024; Received in revised form 1 October 2025; Accepted 5 November 2025
Available online 11 November 2025
2352-0124/© 2025 The Author(s). Published by Elsevier Ltd on behalf of Institution of Structural Engineers. This is an open access article under the CC BY license (http://creativecommons.org/licenses/by/4.0/).

Nomenclature

A	Cross-section area (m^2)
$\overline{A_s}$	Normalised resistance factor in *p-y* spring calculation
A_{sy}	Shear area of cross-section in local y-axis (m^2)
A_{sz}	Shear area of cross-section in local z-axis (m^2)
A_{total}	Total area of the scour zone of influence (m^2)
d_s	Scour depth (m)
D	Pile diameter (m)
E	Elastic modulus (kN/m^2)
G	Shear modulus (kN/m^2)
I_{xx}	Torsional moment of inertia of cross-section (m^4)
I_{yy}	Moment of inertia of cross-section about the local y-axis (m^4)
I_{zz}	Moment of inertia of cross-section about the local z-axis (m^4)
k	Coefficient of subgrade reaction of the *p-y* springs (kN/m^3)
K	Coefficient of lateral earth pressure
N_q^*	Bearing factor of the pile
p_a	Atmospheric pressure (100 kPa)
p_u	Ultimate soil resistance per unit length (kN/m)
P_u	Ultimate force of *p-y* spring (kN)
Q_u	Ultimate force of *q-z* spring (kN)
$T_{s,x}$	Principal vibration period in x- (traffic) direction under scour (s)
$T_{s,y}$	Principal vibration period in y- (flow) direction under scour (s)
T_u	Ultimate force of *t-z* spring (kN)
$T_{0,x}$	Principal vibration period in x- (traffic) direction without scour (s)
$T_{0,y}$	Principal vibration period in y- (flow) direction without scour (s)
$y_{\lim}$	Limiting width of the zone of scour influence (5*D*)
y_s	Scour hole base width (m)
y_{top}	Scour hole top width (m)
y_{50}	Displacements at 50 % of the ultimate force of the *p-y* spring (m)
z	Depth of the spring (m)
$z_{s,eff}$	Effective height of overburden above the scour hole base due to scour hole shape (m)
z_{qz50}	Displacements at 50 % of the ultimate force of the *q-z* spring (m)
z_{tz50}	Displacements at 50 % of the ultimate force of the *t-z* spring (m)
α	Angle of the scour hole (°)
γ	Unit weight (kN/m^3)
Δz	Vertical spacing between *p-y*, *t-z* and *q-z* springs (tributary length) (m)
δ	Friction angle of the soil-foundation interface (°)
σ_v'	Vertical effective stress (kN/m^2)
ϕ'	Angle of friction of the soil (°)
$\phi_{i,0}$	Mode shape vector of the unscoured bridge in *i*th direction of analysis; $i = \{X,Y\}$
$\phi_{i,s}$	Mode shape vector of the bridge under scour in *i*th direction of analysis; $i = \{X,Y\}$

significantly exacerbated under flood conditions [9,10], and can be drastically intensified by debris accumulation [11]. Due to the interdependence on many parameters, accurately predicting scour hole formation remains an active area of research [12].

The removal of soil by scour erosion can lead to reduced stiffness and capacity in bridge foundations. In severe cases, this can result in serviceability failure through excessive settlements, secondary damage such as cracks forming from differential settlements [13], or partial to total bridge collapse [14]. Fig. 1 shows an example of a scour-related bridge failure in Slovenia in 2023. Detecting and quantifying scour occurrence is very important for bridge asset managers.

The most common approach for detecting and monitoring scour is via visual inspection [3], whereby divers physically inspect the condition of foundations at discrete time intervals. This is generally labour-intensive, costly, and subjective. Moreover, it only provides a picture of the scour problem as a snapshot in time and can generally only be conducted once flood conditions have subsided. Therefore, it is of questionable efficacy for scour risk assessments, as scour conditions can change rapidly during a flood, and local scour holes tend to infill when floods subside, masking the issue. To combat this, researchers have developed a range of approaches to reduce or even replace the need for divers, using installed instrumentation that can remotely monitor scour hole development. Examples include float-out devices [3,15,16], radar (and sound pulse) measurement [4,17–20], moving sensors installed on rods in the soil [21,22], and sensors that detect changes in electrical conductivity to locate a scour hole by identifying where the soil level lies

Fig. 1. Example of bridge collapse under scour in Slovenian flood in 2023.

[3,20]. Although this is an improvement on the use of physical divers, many of these sensors can only detect the scour condition local to the sensor and tend not to provide any information on the condition of the bridge due to the presence of a scour hole.

With ever-increasing levels of digitisation and smart monitoring, approaches have been developed to detect scour erosion by monitoring the vibration response of bridge structures under environmental or traffic loading. Vibration-based Structural Health Monitoring (SHM) of bridges is an active area of research. It works on the premise that damage to a structure can alter the fundamental dynamic properties of that structure; and that by measuring these changes, one can deduce the damage condition or extent. Sensors placed on a structure can measure structural accelerations or velocities resulting from external actions such as environmental or traffic loading, and these data can be analysed to derive modal properties such as natural frequency, mode shapes, or damping ratios, for example. Observing changes in these (and other) properties can be used to infer damage. Many researchers have investigated approaches to detecting damage such as cracking in bridge elements by analysing local and global dynamic behaviour (e.g. [23–27]).

The application of vibration-based SHM to detecting scour has gained significant traction in recent years. Scour effectively leads to a change in stiffness at the bridge foundation, which manifests as a change in the dynamic properties of the structure [28]. The most commonly investigated vibration-based SHM approach for scour detection relates to detecting changes in the natural frequency, arguably the simplest of the modal parameters to measure. Prendergast et al. [29] investigated the change in frequency of a single foundation pile under scour and developed a simple Winkler-beam model [30,31] to track the frequency change, with the soil properties informed from geotechnical test data. Scour was modelled as the incremental removal of springs from the Winkler model to simulate the action of soil erosion. The approach was extended to assessing if scour could be detected around a bridge foundation by developing a vehicle-bridge-soil interaction model and simulating excitation from passing vehicles [32–34]. It was concluded that excitations from passing vehicles could be used to determine if scour existed at a given foundation by analysing the first natural frequency of the bridge response [32], and also which foundation (in multi-foundation bridges) was affected by analysing different modal frequencies and sensor locations [33]. Kong and Cai [35] investigated how scour erosion affected the response of a bridge under a traversing vehicle in the presence of wave loading on the substructure, and concluded that scour significantly influenced the natural frequencies of the bridge pile. Chen et al. [36] investigated how scour affecting the pylon support of a cable-stayed bridge could be detected by analysing the local natural frequencies of the pylon and varying the soil level in a numerical model to determine the scour depth. Ju [37] created a three-dimensional numerical model of a bridge and investigated how scour influenced the natural frequencies in the presence of water-added mass. They note that the change in frequency with scour is not smooth due to non-uniform foundation elements. [38]. Other authors have investigated various approaches to detecting and monitoring scour, such as: mode shape-based methods [38–42]; flexibility-based deflections [42,43]; and offline methods using the response of passing vehicles to detect the presence of scour damage [44,45].

One issue that remains broadly unresolved is how much of a behaviour change, e.g., a change in natural frequency or mode shape, needs to occur to indicate if a scour problem exists with a given bridge structure. A key challenge is determining thresholds for these changes in dynamic properties that signal significant structural risk. Moreover, little research has focussed on how different scour hole shapes might affect the dynamic behaviour of a given bridge, and the resulting impact on the magnitude of changes that need to occur to indicate the presence of damage. Bao et al. [46] investigated how the shape of a scour hole (whether symmetrical or asymmetrical) affected the measured natural frequency of a single-pier model under scour. The scour shape effect was considered by imposing different scour levels (depths) on either side of the modelled pier. Frequency was observed to reduce with scour, and the effect of the asymmetrical scour shape was to change the magnitude of the detected frequency at a given scour depth. The research was applied to a single free-ended pier model, so the bridge superstructure's additional interaction was not considered. This leaves a gap in understanding how complex bridge structures might behave under similar scour conditions. Other authors have focussed on the lateral deflections of individual piles under different scour conditions. Lin et al. [47] investigated how scour affects the lateral loading response of piles in sand, considering the change in soil stress history due to the occurrence of the scour hole. The soil stress history changes from normally-consolidated to over-consolidated as a result of the scour occurrence removing overburden. By considering this stress history, the remaining soil below the scour level exhibited an increased lateral resistance for the over-consolidated case, which resulted in lower lateral deflections in the pile than observed in the model where stress history was not considered. The authors conclude that ignoring the effects of stress history, i.e. the increased resistance generated, is conservative for lateral pile design. Zhang et al. [48] investigated the influence of scour hole shape and changes in soil stress history on the response of laterally-loaded piles in clay. They show that total removal of a soil layer, i.e. general scour, leads to lower soil resistance in the remaining soil than in the case where the scour hole geometry is considered. Moreover, they note that scour depth has the largest influence on the response among the various scour hole dimensions (e.g. scour depth, scour width, scour-hole slope angle). Lin et al. [49] undertook a similar analysis for laterally-loaded piles in sand considering scour hole shape dimensions. A simplified method was adopted to modify lateral load-displacement *p-y* models to account for the three-dimensional scour hole geometry. Similar to Zhang et al. [48], the authors concluded that scour depth is the most influential scour dimension affecting the lateral response, and considering the presence of the scour geometry leads to a reduction in the predicted lateral displacement of a pile compared to the case where the entire soil layer is considered to be removed. The same authors investigated the lateral response of piles in clay considering scour-hole dimensions [50], and concluded that ignoring the scour-hole geometry leads to larger deflections than occur if the scour geometry is explicitly considered. A lot of ongoing research in this area is focussed on offshore structures such as wind turbine foundations, in addition to bridge foundations, offering novel insights to scour effects on structures [51–58].

While there has been some encouraging research focussing on the response of single piles to scour considering the scour hole geometry, limited research has focussed on the modal responses of a full bridge when scour hole geometry is taken into account. Tubaldi et al. [59] performed experimental and numerical studies on the effect of scour hole shapes on the dynamic properties of bridges with shallow foundations. The study investigated various modelling approaches for the soil-foundation-structural system as informed from testing on a structural prototype. Results indicate that frequencies of vibration of the bridge were observed to decrease linearly with increasing scour hole width. However, the analyses did not consider bridges with piled foundations. This is crucial to understand as the influence of scour hole geometry on the behaviour of piled bridges is likely to affect the performance of vibration-based SHM approaches tasked with detecting the presence of scour. Moreover, there is limited practical guidance on how to consider scour hole shapes in routine analyses of bridges on piles, impacting the ability for asset managers to link changes in SHM parameters to underlying scour conditions. This paper addresses these gaps and investigates how differently shaped scour holes might impact the vibration characteristics of an example bridge structure; specifically how modal frequencies are affected for different scour hole shapes. The purpose of the study is to highlight the potential complexity of detecting and quantifying scour occurrence using vibration-based approaches under variable scour conditions. The bridge model developed in Kosič et al. [11] is enhanced to consider a pile group foundation affected by

scour erosion with different scour hole shapes. A simplified, novel, practice-oriented method is developed to consider the contribution of soil overburden stresses from various shapes of scour holes in sand, and the resulting influence on the foundation stiffness and strength. Scour hole shapes are varied to consider local scour (with hole widths varying from narrow to wide) [60,61], as well as general scour (full removal of a soil layer), and the impact on the change in the bridge dynamic characteristics is assessed, and contextualised for the use of structural health monitoring systems.

2. Bridge model

2.1. Description of bridge

The bridge model developed in Kosič et al. [11] is considered in this paper, with an enhancement to the foundation for the purpose of assessing scour hole shape effects. The bridge is based on a girder bridge spanning the Kupa river in Croatia, with two main spans. Each span is 48.6 m in length, supported on a central pier. The bridge width is 12.4 m, supporting two traffic lanes and a cantilevered pedestrian zone. The main geometrical and material properties are provided in Table 1, and Fig. 2 shows a schematic of the bridge. Table A1 in the appendix provides more detailed information on the properties of the bridge elements.

The central pier is considered to be supported on a 1.0 m deep pilecap, founded on six piles. The pile dimensions have been designed for the purpose of the analysis in this paper, whereby a factor of safety (FoS) of 2 is adopted against axial capacity failure. Three soil profiles are considered: a loose sand, a medium-dense sand, and a dense sand profile. The pile design is conducted according to Meyerhof's [62] method for axial capacity. The resulting pile dimensions are provided in Table 2 for the three soil profiles considered. The purpose of using different pile geometries is to investigate the impact of different scour geometries on the modal properties of a bridge, for a given foundation where the same FoS is considered for each. Note, while the superstructure of the bridge is based on a real structure, the foundation model is developed solely for the analyses in this paper. Hence, the bridge is not considered to model any particular structure.

2.2. Numerical modelling

A numerical model of the roadway bridge is developed in OpenSees software [63,64]. The structural modelling, soil-structure interaction, and scour modelling approaches are presented herein. A schematic of the modelled bridge is shown in Fig. 3, showing the boundary conditions, foundation schematic, and the soil modelling framework adopted. Table A1 in the appendix provides detailed material and geometrical properties of the model. Fig. 3 also schematically shows the different scour shape scenarios considered; namely local narrow scour, local wide scour, and general scour, affecting the foundation. Note that the global coordinate axis (X,Y,Z) is used to reference the directions with regard to the modal behaviour in this paper. A local coordinate axis is used for the

Table 1
Geometry and material properties of the modelled bridge.

Element	Property	Base material	E (kN/m^2)	G (kN/m^2)	γ (kN/m^3)
Deck	Composite section	Steel	2.10E+ 08	8.08E+ 07	77
Pier	Rectangular section	Concrete	3.10E+ 07	1.29E+ 07	25
Stiff*	-	-	2.10E+ 14	8.08E+ 13	0
Foundation	Circular section	Concrete	3.10E+ 07	1.29E+ 07	25

* Stiff and weightless element used to provide connectivity in numerical model

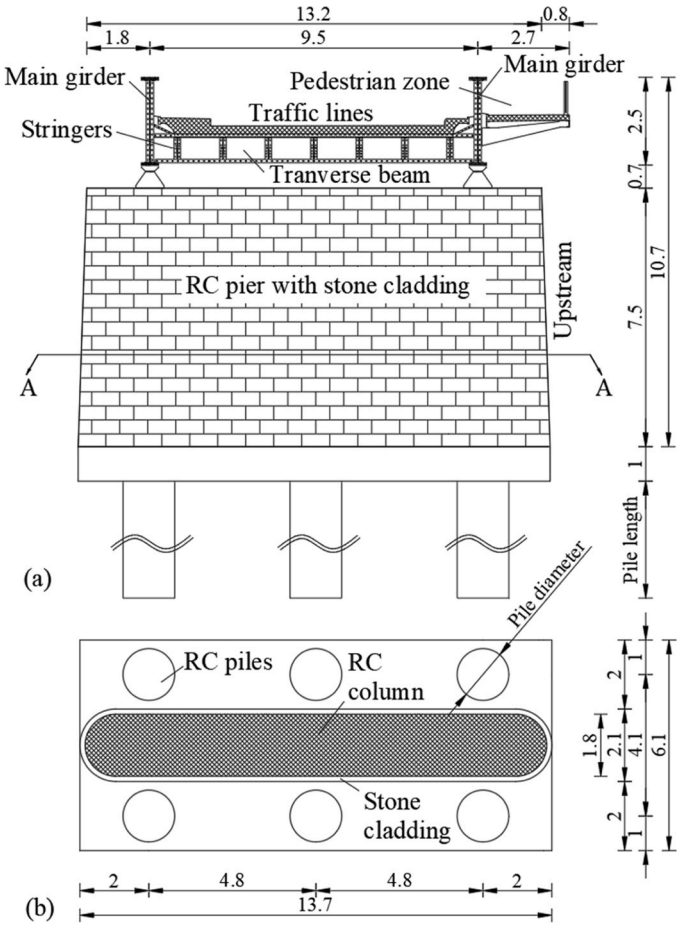

Fig. 2. Schematic of the model bridge (modified after Kosič et al. [11], dimensions in m).

Table 2
Pile geometries for each soil type (resulting in same FoS for each model).

Soil profile	Pile diameter (m)	Pile length (m)
Loose sand	1.5	16
Medium-dense sand	1.0	12
Dense sand	0.8	8

soil-structure interaction to remain in keeping with the terminology used in that field, i.e. the lateral springs are referred to as lateral load (p)-lateral displacement (y) regardless of the horizontal direction in which they act. Horizontal springs are considered to act in both the X and Y directions, with vertical springs acting in the Z direction.

2.2.1. Structural modelling

The superstructure and foundations of the bridge are modelled using linear elastic Timoshenko beam-column elements, with elemental mass and stiffness matrices as available in Kwon and Bang [65]. The bridge deck is modelled using an equivalent beam element and is considered to be supported on bearings. Variation in stiffness of the deck due to changing thicknesses of the main girder flanges is considered using an array of beam elements with varying properties. The central pier is modelled in a similar manner. A long stiff element is used to model the pilecap, and six piles are modelled using an array of discrete elements along their depths. Each element is considered to be 0.1 m in length. Roller bearings are used at the bridge boundaries to model free translation behaviour of the deck sitting on rigid abutments.

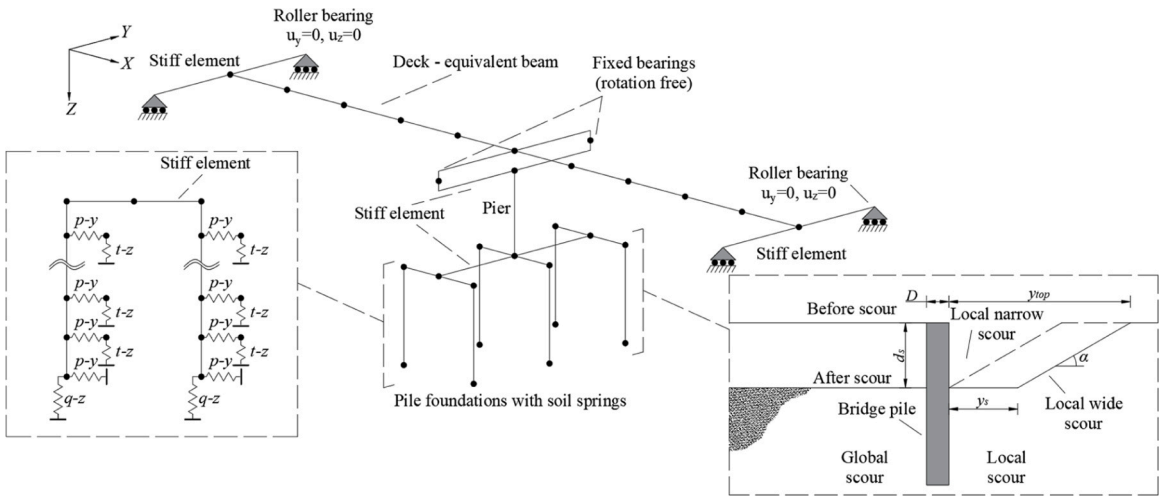

Fig. 3. Numerical schematic of the modelled bridge.

2.2.2. Soil-structure interaction (SSI)

The soil-structure interaction is considered using a Winkler-beam framework [30,31], by means of lateral load-displacement *p-y* springs, vertical shear stress-displacement *t-z* springs, and a vertical base resistance-displacement *q-z* spring, see the insert in Fig. 3. The springs are incorporated into the OpenSees model using *ZeroLength* elements, which connect the pile nodes to fixed nodes to represent the connection with the ground. The load–displacement behaviour of the *p-y*, *t-z* and *q-z* springs is modelled using OpenSees uniaxial material *PySimple1* [66], *TzSimple1* [67] and *QzSimple1* [68], respectively, for each resistance mechanism, described below. These functions require input parameters, namely ultimate force values (P_u, T_u, Q_u) and respective displacements at 50 % of the ultimate force (y_{50}, z_{tz50}, z_{qz50}), for each spring type.

The lateral load-displacement *p-y* backbone curve was derived according to the API code [69], with the ultimate resistance (P_u) computed according to Reese and Van Impe [70], as follows:

$$P_u = \overline{A_s} p_u \Delta z \tag{1}$$

where $\overline{A_s}$ is the normalised resistance factor, which is a function of the ratio $\frac{z-d_s+z_{s,\text{eff}}}{D}$ (z is the depth of the spring relative to the original ground level, d_s is the scour hole depth, $z_{s,\text{eff}}$ is the effective height of overburden above the scour hole base due to scour hole shape [derivation provided in Section 2.2.3], D is the foundation diameter); p_u is the ultimate soil resistance per unit length [70]; and Δz is the vertical spacing between soil springs. The displacement at 50 % of the ultimate load is calculated based on the API [69] hyperbolic load-displacement curve:

$$y_{50} = \frac{\overline{A_s} p_u}{k(z - d_s + z_{s,\text{eff}})} \text{atanh}(0.5) \tag{2}$$

where k is the coefficient of subgrade reaction, which is a function of soil density (or friction angle), and varies depending on whether conditions are saturated or unsaturated.

The vertical shear stress-displacement *t*-z backbone curve is described as a bilinear (Mohr-Coulomb) curve, with the ultimate resistance derived as follows [71]:

$$T_u = K\sigma_v' \tan(\delta)\pi D \Delta z \tag{3}$$

The coefficient of lateral earth pressure is assumed as K= 1.0 for full displacement piles, σ_v' is the vertical effective stress (including the contribution from the overburden at the scour hole – see Section 2.2.3), and δ is the soil-pile interface friction angle, specified as $0.9\phi'$ (where $\phi'$is the angle of friction of the soil). The displacement at 50 % of the ultimate load (z_{tz50}) is taken as 1.27 mm [72].

The vertical base resistance-displacement *q-z* backbone curve is defined according to the Vijayvergiya's [73] recommendations with the ultimate tip bearing resistance of the pile computed according to Meyerhof [62]:

$$Q_u = \left[\sigma_v' N_q^*\right]\pi\frac{D^2}{4} \le \left[0.5 p_a N_q^* \tan(\phi')\right]\pi\frac{D^2}{4} \tag{4}$$

where N_q^* is the bearing factor of the pile, and p_a is atmospheric pressure (100 kPa). The displacement at 50 % of the capacity (z_{qz50}) is assumed as 12.5 % of the pile ultimate displacement [73]. The latter is assumed to be attained at the displacement equal to 5 % of the pile diameter (0.05D).

2.2.3. Scour hole modelling

A practical and simplified scour modelling approach is proposed that can account for differently-shaped scour holes. The method is intended to be used in conjunction with Winkler modelling approaches for SSI, which are popular in industry (see Section 2.2.2). Scour is modelled by removing springs from the model to simulate the action of water eroding soil [32,33], with the properties of the remaining springs adjusted to account for scour hole shape variations (different depths, widths, and slope angles). To account for the presence of overburden, an effective depth is considered, which takes into account the extra overburden that exists above the base of the scour hole for different scour hole shapes. This effective depth, $z_{s,\text{eff}}$, is considered to act above the base of the scour hole, shown schematically in Fig. 4, to account for the overburden presence. Different types of scour are considered, ranging from local narrow and local wide scour, to general scour. Narrow scour refers to the scour hole being immediately adjacent to the foundation, wide scour assumes a flat base to the scour hole around the foundation, and general scour refers to complete layer removal or the scour hole being wider than the zone of influence around the foundation. Local narrow, wide, and general scour cases are shown schematically in the inset in Fig. 3. The distance around the foundation where the overburden is considered to have an influence is assumed as 5D away from the foundation, conservatively larger than the value of 4 suggested in other studies [74]. The effective depth accounting for the influence of overburden is derived by assuming a wedge of soil within the zone of influence acting as a proportion of the total soil area that would exist in the absence of scour. Four cases can occur, as elaborated in Fig. 4.

Fig. 4(a) and (b) demonstrate the case where a local narrow to wide scour hole forms, without and with a base width y_s, whereby the top width y_{top} is less than the limiting width of the zone of influence y_{lim}. The area of the wedge of soil within the limiting distance is calculated using:

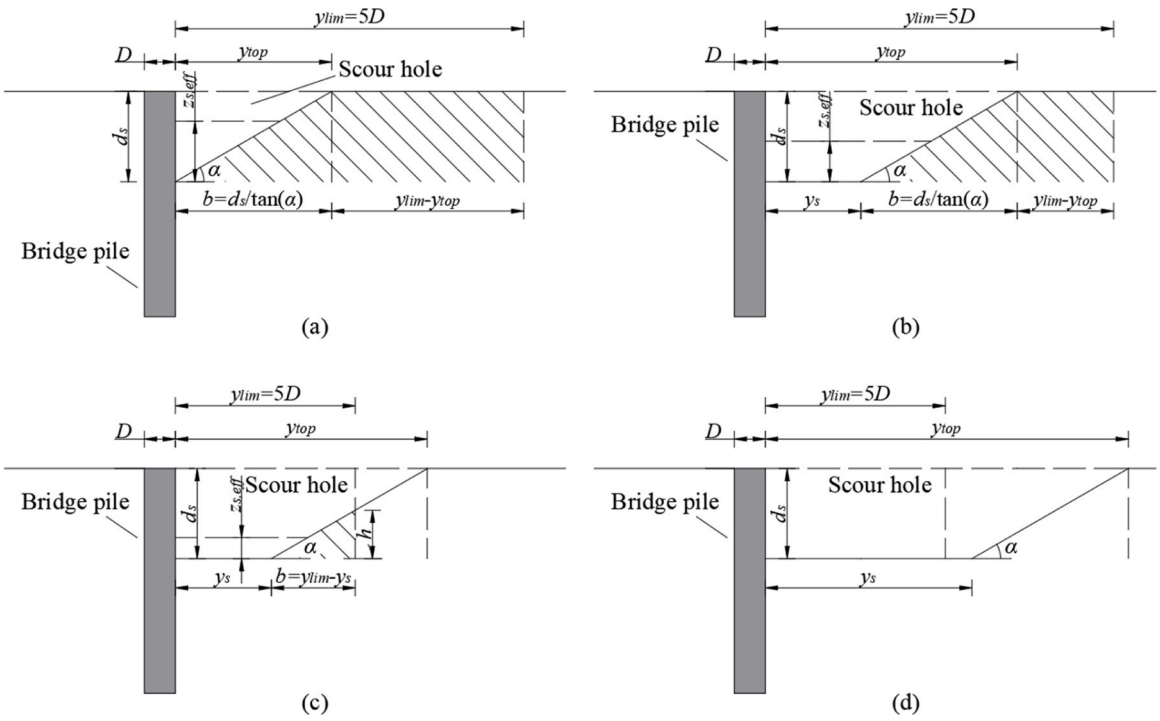

Fig. 4. Scour overburden derivation, (a) Local narrow scour: top of scour hole width less than zone of influence (large soil wedge contributes overburden) with no scour hole base width, (b) Local wide scour: top of scour hole width less than zone of influence with bottom scour width included (large soil wedge contributes overburden), (c) Local wide scour: top of scour hole width exceeds zone of influence but bottom of scour hole width within zone of influence (small soil wedge contributes overburden), (g) General scour: bottom of scour hole width exceeding zone of influence (no overburden contribution).

$$A_{soil} = 0.5bd_s + \left(y_{\lim} - y_{top}\right)d_s \tag{5}$$

The total area of soil that would exist in the same limiting distance in the absence of scour is calculated as:

$$A_{total} = y_{\lim}d_s \tag{6}$$

The effective overburden depth to be added to the scour hole base, as a function of the scour depth, is calculated as:

$$z_{s,\mathrm{eff}} = \frac{A_{soil}}{A_{total}}d_s \tag{7}$$

$z_{s,\mathrm{eff}}$ is included in the calculation of effective stress or ultimate resistance in the derivation of the parameters for the soil springs described in Section 2.2.2. Fig. 4(c) presents the case of wide local scour where the top width of the scour hole exceeds the limiting distance, while the bottom width does not, resulting in a smaller wedge of soil contributing to the overburden influence in the calculations. In this case, A_{soil} is calculated as:

$$A_{soil} = 0.5(y_{\lim} - y_s)h \tag{8}$$

where $h = (y_{\lim} - y_s)\tan(\alpha)$, and α is the angle of the scour hole. $z_{s,\mathrm{eff}}$ is then derived using Eq.(7). Fig. 4(d) demonstrates the case where the scour hole bottom width is larger than the zone of influence, resulting in no effective overburden being added to the calculation of effective stress, i.e. $z_{s,\mathrm{eff}} = 0$.

The calculations consider the problem as a 2D area ratio. This simplification is adopted as it is assumed an approximately circular scour hole in 3D would result in the same volume ratio of soil overburden to total soil volume in the absence of scour. Moreover, as *p-y*, *t-z*, and *q-z* springs inherently consider the SSI in a plane-strain manner, it is sensible to derive the additional overburden as an equivalent effective depth of soil using the above approach. The modifications to the SSI parameters to account for scour hole shape inherently assume the scour depth is uniform across the foundation. While scour depth tends to vary between the upstream and downstream end of a given foundation in real cases, the implementation of uniform scour can be considered as a representative mean scour condition affecting a given foundation. Moreover, Winkler springs are implemented in the model in both the global *X* and *Y* directions, hence the scour hole properties are considered the same in both directions for this case. It should be noted that while the SSI implemented in this paper follows the API code [69], the effective depth to account for scour hole overburden can be implemented into any Winkler-type SSI model, provided an estimate of depth or effective stress is required in the spring derivation. Non-uniform or layered soil profiles can be considered in this manner.

3. Analysis and results

In this section, the influence of the shape of scour holes on the modal periods and mode shapes of the modelled bridge are presented, discussed, and contextualised in the frame of structural health monitoring applications. Different scour hole shapes are considered by varying the depth and width of scour holes.

3.1. Influence of scour hole shape on modal periods

Using the procedure to calculate an effective overburden contribution to the strength and stiffness of the soil springs below a scour hole for varying scour hole shapes, the influence of differently-shaped scour holes on the modal periods of the bridge is presented herein. A given model is created with an imposed scour depth, width, and slope angle, and modal periods are derived in the model by performing an Eigenanalysis with small-strain properties of the soil springs adopted, i.e. the small-strain stiffness of the respective soil springs are used at the operational strain level of the springs under the imposed bridge loads. Figs. 5–7 show the impact of different scour conditions on the relative change in principal vibration periods of the bridge in the longitudinal (traffic, *X*) and transverse (flow, *Y*) directions for different soil

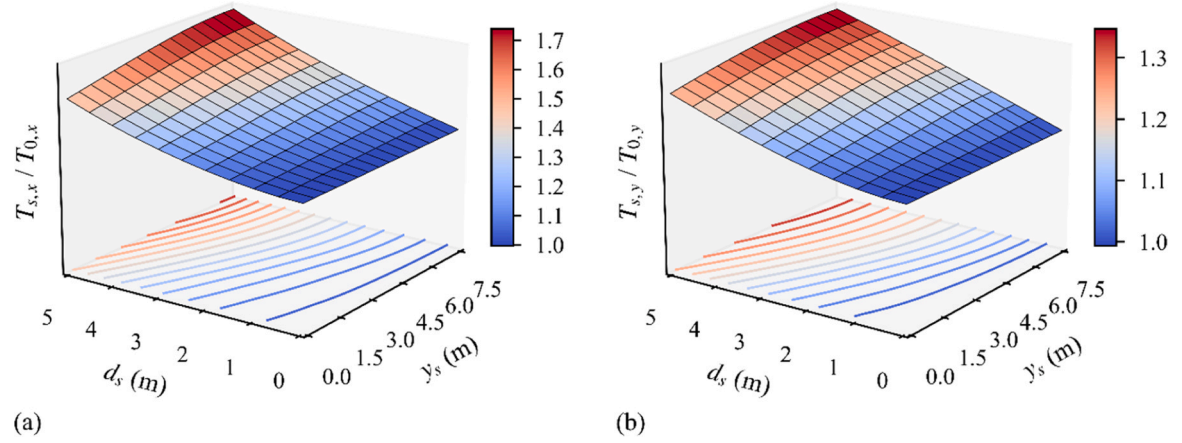

Fig. 5. Impact of scour depth (d_s) and width (y_s) on the relative increase of principal vibration periods (T) in (a) traffic, and (b) flow direction – loose soil profile (pile length 16 m, diameter 1.5 m). Subscripts s = scoured, 0 = unscoured.

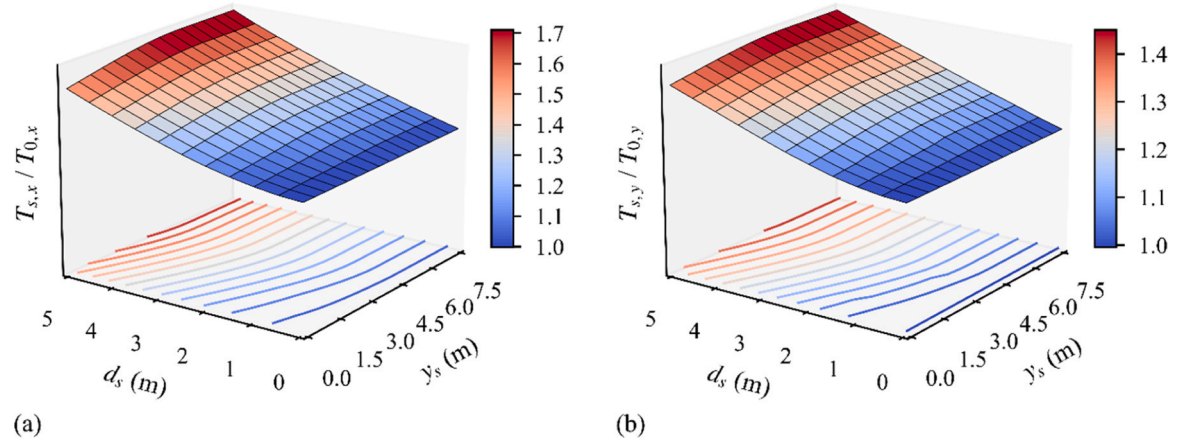

Fig. 6. Impact of scour depth (d_s) and width (y_s) on relative increase of principal vibration periods in (a) traffic, and (b) flow direction – medium dense soil profile (pile length 12 m, diameter 1.0 m).

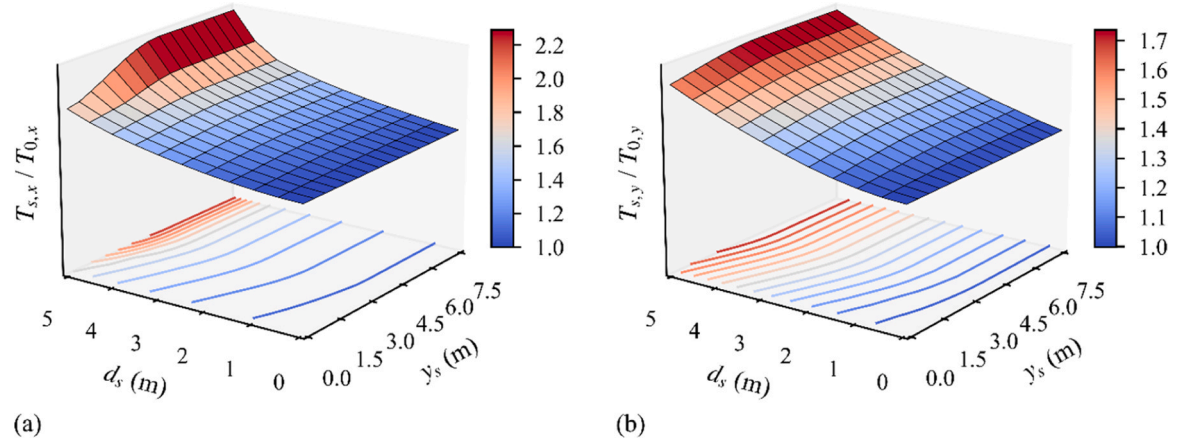

Fig. 7. Impact of scour depth (d_s) and width (y_s) on relative increase of principal vibration periods in (a) traffic, and (b) flow direction – dense soil profile (pile length 8 m, diameter 0.8 m).

conditions (loose, medium-dense, and dense soil profiles), respectively. These plots are generated by creating a range of models with varying scour depths and widths, and plotting the resulting modal periods from the Eigenanalyses. In total, 176 simulations were run (scour depths 0 m to 5 m in 0.5 m steps, and scour width 0 m to 7.5 m in 0.5 m steps, with constant slope angle of 30°) to create the data in Fig. 5, for example. Regardless of the soil type, the presence of scour increases the vibration periods in both traffic and flow directions due to the decreased foundation stiffness under scour, a well-known result observed in many previous studies. For a given soil profile and vibration direction, the modal period increases with an increase in scour depth, d_s. However, there is also an increase evident with scour hole width, y_s, due to the

change in overburden contribution. Wider scour holes contribute less overburden than narrower scour holes. For smaller scour depths, the influence of the scour hole width is less significant than at larger scour depths. Asymptotic (plateau) behaviour is evident at larger scour depths, whereby as scour hole width increases progressively from narrow to wide, there is a larger increase in modal period than for cases with wider (towards general) scour. This is particularly evident in Fig. 7 (a) for a scour depth of 5 m, whereby the modal periods increase much more for lower scour width values than for larger ones.

The increase in modal period is larger in the traffic direction compared with the flow direction in the considered bridge model. This is a result of the traffic direction having lower stiffness as a result of the pile arrangement (i.e. this is the weaker structural axis for the bridge modelled). In this direction, the horizontal stiffness of the bridge is provided only by cantilever action of the pier, as the abutment connections are on roller bearings. The impact of the scour is smaller in the flow direction due to the larger foundation dimensions and additional stiffness provided by the deck. This trend can be seen by comparing the '(a)' plots in Figs. 5–7 with the '(b)' plots, noting the magnitude of the change on the colour bar in each plot.

By comparing Figs. 5–7 the relative impact of scour differs for the three soil profiles. This is a result of the different pile dimensions used to satisfy the axial pile design, i.e. each bridge has the same FoS against axial capacity failure (FoS = 2), resulting in different pile lengths for each soil density, see Table 2. Scour has the largest impact on the dense soil profile, Fig. 7 (smallest pile length), with lower impacts for the medium-dense, Fig. 6, and loose sand, Fig. 5, profiles (longer pile lengths).

Figs. 8 and 9 show the same data as in Figs. 5 and 6, condensed to two dimensions to facilitate a comparison of the behaviour. For the loose soil profile in Fig. 8, the relative change in vibration periods in both directions increases smoothly with an increase in d_s and y_s. The same behaviour is evident for the medium-dense sand profile in Fig. 9, but only for the case of the vibration periods in the traffic (longitudinal) direction (Fig. 9a). In Fig. 9(b), for the flow (transverse) direction, a non-smooth transition is observed for two specific scour conditions, namely $\{d_s, y_s\} = \{1.0\text{ m}, 3.5\text{ m}\}$ and $\{d_s, y_s\} = \{1.5\text{ m}, 1.5\text{ m}\}$. This non-smooth change with scour indicates a fundamental change in the modal behaviour of the bridge under specific circumstances. Examining the bridge mode shapes indicates that for these specific scour conditions in this bridge arrangement, the predominant transverse and vertical vibration periods align, resulting in coupling between these specific mode shapes. This mobilises a distinct mode shape, which does not occur in the unscoured bridge. The impact of varying scour conditions on the change in mode shapes is further examined in the next section (Section 3.2). The data for the dense sand profile are presented in Appendix B.

3.2. Influence of scour hole shape on mode shapes

The impact of scour hole shape (varying depth and widths) on the change in mode shapes of the bridge is examined herein. Similar to the modal periods, the mode shapes are derived by performing an Eigenanalysis at the operational strain level of the soil springs under the imposed loads. To effectively track the change of the bridge's mode shapes for different scour conditions, the Modal Assurance Criterion (MAC) is used, which quantifies the degree of consistency or correlation between mode shapes, allowing a measure of linearity between two modes be established [75]. MAC is defined as:

$$\mathrm{MAC}(\phi_{i,0}, \phi_{i,s}) = \frac{\left|\phi_{i,0}^T \phi_{i,s}\right|^2}{\left(\phi_{i,0}^T \phi_{i,0}\right)\left(\phi_{i,s}^T \phi_{i,s}\right)};\ i = \{X, Y\} \tag{9}$$

where $\phi_{i,0}$ and $\phi_{i,s}$ represent the mode shape vectors of two states, e.g., the benchmark model (0) and the model with scour (s), while the index i represents the direction of analysis. The MAC value ranges between 0 and 1, with a value of 1 indicating perfect correlation and 0 indicating no correlation. In the present study, MAC is applied to assess the similarity between the mode shapes of the benchmark finite element model (representing the bridge under the no-scour condition) and those of comparative numerical models with varying scour conditions modelled. The impact of different scour depths and widths on the dynamic behaviour of the bridge can be evaluated in this way, facilitating a deeper understanding of how scour-induced changes affect structural modal properties.

Figs. 10 and 11 present the change in MAC values between the unscoured bridge modes and the scoured bridge modes for various scour conditions in the (a) traffic, and (b) flow directions, for loose and

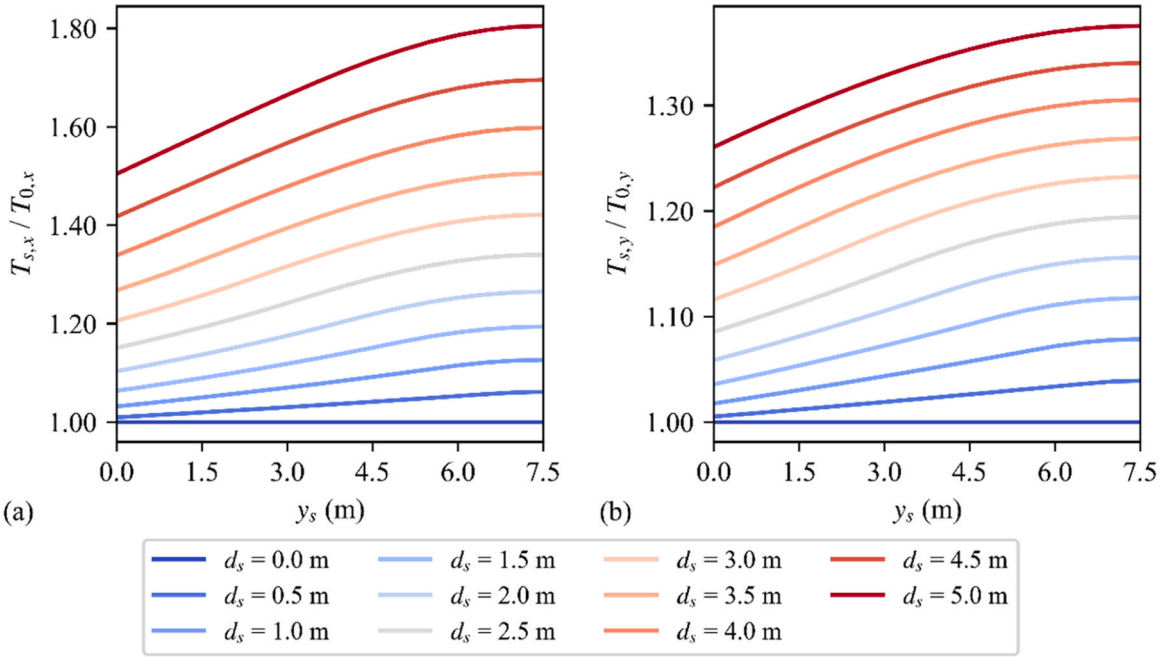

Fig. 8. Relative change of global vibration period in (a) traffic, and (b) flow direction for different scour depths (d_s) and widths (y_s) – loose soil profile.

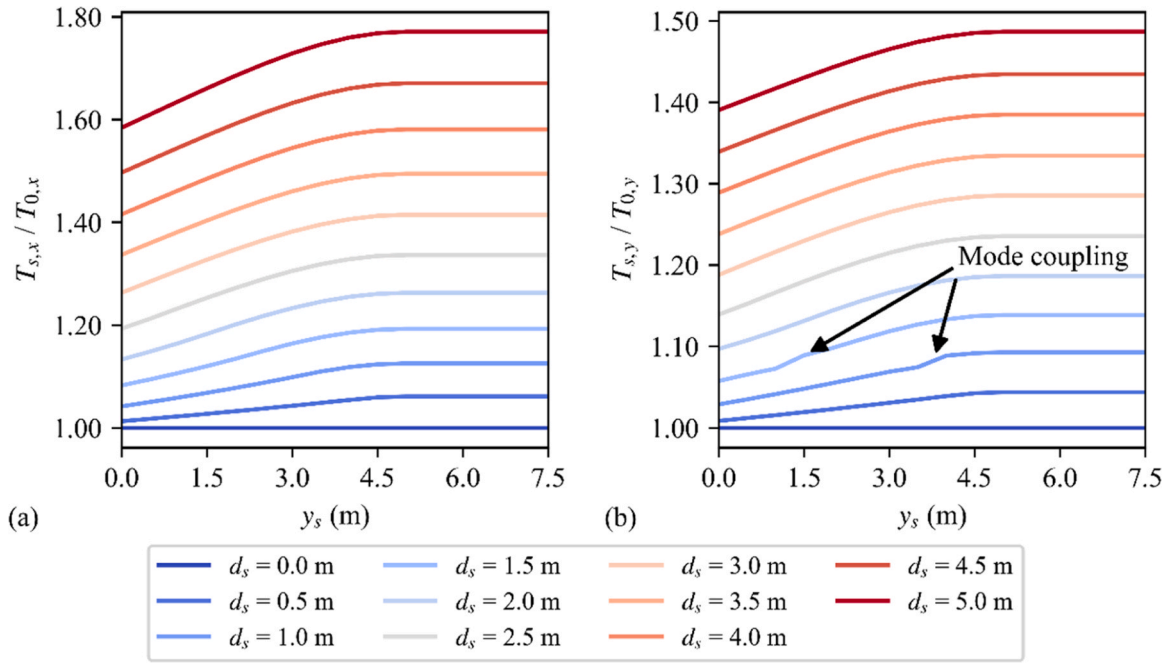

Fig. 9. Relative change of global vibration period in (a) traffic, and (b) flow direction for different scour depths (d_s) and widths (y_s) – medium dense soil profile.

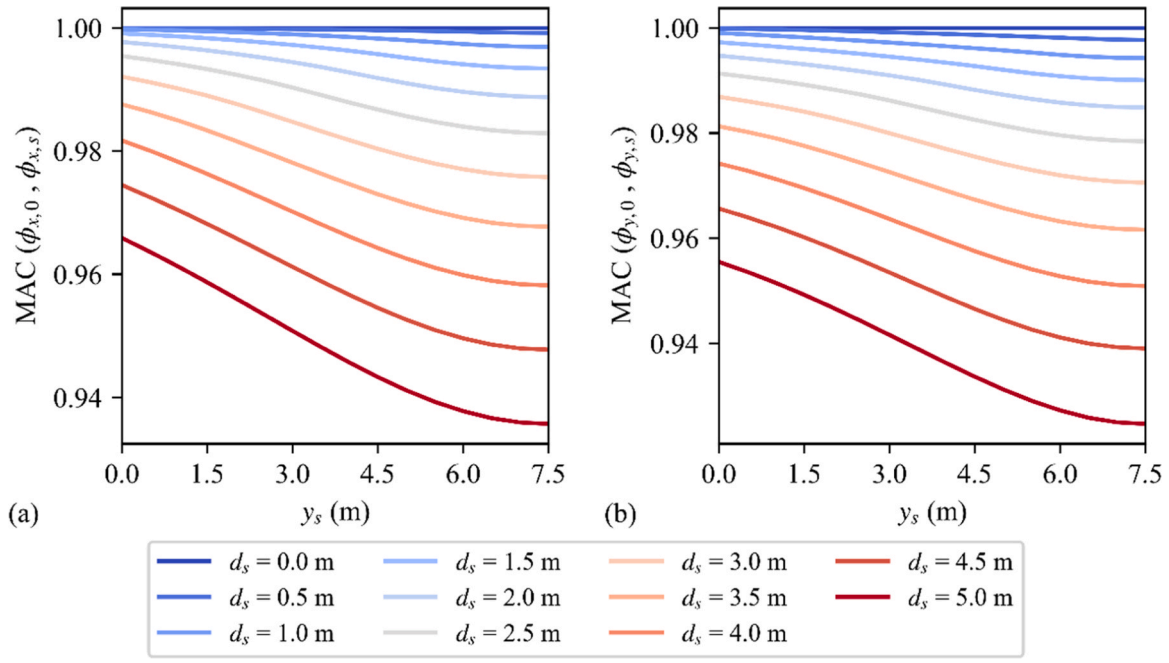

Fig. 10. MAC values of the (a) traffic, and (b) flow direction mode shape under different scour conditions, benchmarked against the mode shape of the unscoured bridge – loose soil profile.

medium-dense soil profiles, respectively. In Fig. 10(a) and (b), the MAC value is observed to reduce as scour depth, d_s, increases. Moreover, for a given scour depth, the MAC value further reduces as the scour width, y_s, is increased. For larger scour hole widths, the influence reduces, as shown by the asymptotic behaviour of each line as scour widths increase to large values approaching general scour. This analysis suggests that the change in the bridge boundary condition due to scour leads to a smooth change in the MAC as the scoured bridge mode deviates away from the unscoured bridge mode. This finding is as expected, in that the gradual softening of the bridge boundary constraint under increasing scour depth and width leads to a smooth change in the mode shapes for the first modal periods in the traffic and flow directions.

Fig. 11(a) shows a similar behaviour to that in Fig. 10(a), except that for the medium-dense soil (with the correspondingly shorter pile), the influence of scour is larger with a greater change in the MAC values observed for a given scour depth. Moreover, the plots level off at smaller scour width values as the scour width approaches general scour (5D), for this denser soil profile (and smaller diameter pile).

In Fig. 11(b), which shows the change in MAC value between unscoured and scoured bridge modes in the flow direction for medium-dense soil, a non-smooth transition in MAC value with the progression of scour width is observed for certain scour hole widths. This is a result of the

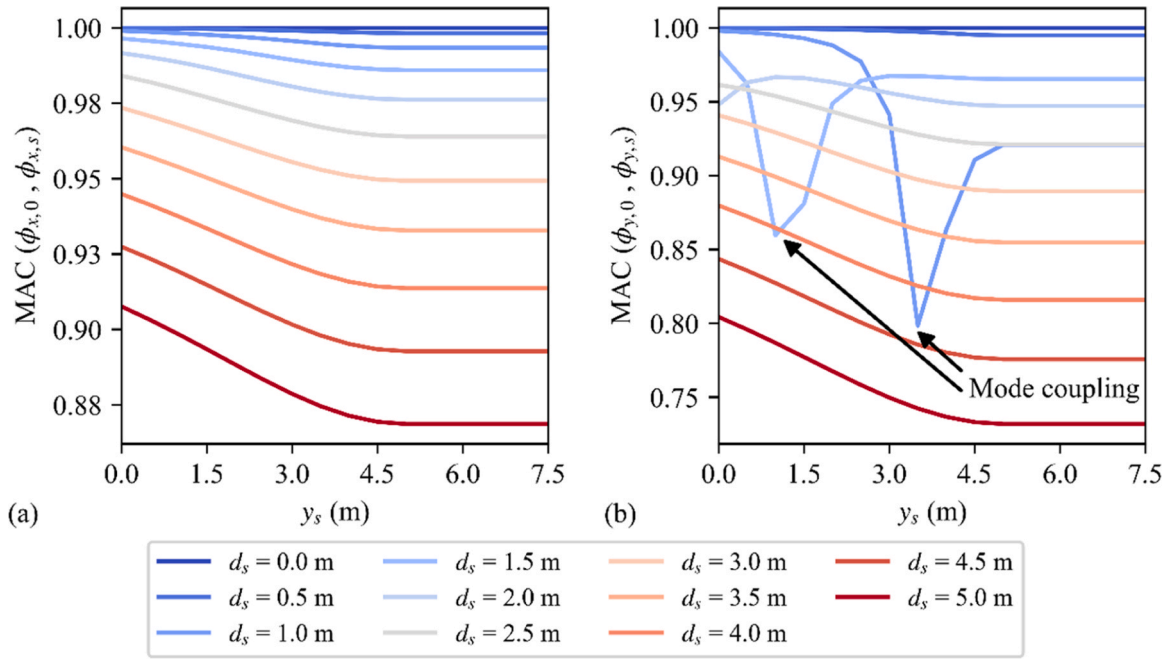

Fig. 11. MAC values of the (a) traffic, and (b) flow direction mode shape under different scour conditions, benchmarked against the mode shape of the unscoured bridge – medium dense soil profile.

mode coupling phenomenon observed in Fig. 9(b), which results from the predominant transverse and vertical vibration periods aligning for the given scour conditions, resulting in a significant change in the MAC value at these specific conditions. The data for the dense sand profile are presented in Appendix B.

The principle of mode coupling at specific scour conditions is illustrated in Fig. 12, where the mode shapes of the unscoured bridge are compared to those of the scoured bridge for two specific scenarios in the bridge model with a medium dense soil profile. Each subfigure shows a three-dimensional mode shape of the bridge, with a colour bar to indicate the magnitude of modal displacement across the structure, from minimum (blue) to maximum (red).

In the first scenario, scour depth (d_s) is set to 1.0 m, while in the second scenario, d_s is increased to 3.0 m. Scour width (y_s) is then set to 3.5 m for both scenarios to demonstrate the mode coupling phenomenon. Fig. 12(a-c) shows the mode shapes of the bridge in the traffic, flow, and vertical directions for the case where no scour affects the bridge. Fig. 12(g-i) shows the mode shapes of the bridge in each direction when the scour hole depth is 3.0 m, and the scour hole width is 3.5 m. The mode shapes are similar in shape to those in Fig. 12 (a-c), with only minor variations, in line with the results in Fig. 11(b) for the 3 m scour depth. As expected, the modal periods increase more for the 3 m scour depth in Fig. 12(g-i) than for those of the 1 m scour depth in Fig. 12(d-f).

The mode shapes in Fig. 12(d-f) are quite different from those in Fig. 12(a-c) in a given direction. Comparing Fig. 12(b), (e), and (h), one would expect to see the mode shape gradually change as the modal period increases for increasing scour. Instead, the mode shape for the 1 m scour depth in the flow direction differs from that of no scour and 3 m scour. This demonstrates visually the mode coupling effect for specific scour depths, and shows why the MAC values in Fig. 11(b) exhibit a non-smooth change with increasing scour width for specific scour depth values. The flow direction and vertical direction modes become coupled for these conditions as the modal periods closely align; note the modal periods are 0.404 s and 0.408 s for these scour conditions in the flow and vertical directions, respectively. This finding highlights a potential complexity with regard to scour monitoring using changes in modal periods or frequency for complex structures. The data in Fig. 12 demonstrates the phenomenon for the scour combination {d_s, y_s}= {1.0 m, 3.5 m}. The same coupling occurs for the {d_s, y_s} = {1.5 m, 1.5 m} case.

The previous analysis highlights the complexity with regard to monitoring scour erosion progression using data-driven vibration-based methods that rely on detecting changes in modal periods or mode shapes of a scoured bridge. For certain scour hole depths or widths affecting complex structures, it is possible that mode shapes may become coupled, which would mask the true scour condition, potentially suggesting that the scour issue is worse than expected, i.e. a sudden change in MAC value between unscoured and scoured modes might suggest a problem when one does not exist. This highlights the significant difficulty with using purely data-driven approaches, whereby damage is evaluated by benchmarking data from the damaged system with that of the healthy system without reference to a numerical model that could shed insight to the behaviour. Conversely, the study highlights the importance of having accurate reference models to benchmark data and understand system behaviour, suggesting model-based structural health monitoring is still very important in an increasingly data-driven industry. The key is to balance data-driven innovations with rigorous model-based validations, ensuring more reliable and actionable insights in understanding complex soil-structure interaction behaviour.

4. Conclusions

In this paper, a simplified and practical method is proposed to modify Winkler-type springs used in SSI to account for the shape of a scour hole affecting a piled bridge. The scour hole shape is considered by applying an effective overburden depth to account for the additional soil strength and stiffness that would exist beneath a scour hole for different types of scour; from local narrow scour to local wide scour; and general scour, where the full soil layer is removed. The effective overburden is calculated as the volume of soil within a zone of influence that contributes effective stress to the soil beneath the scour hole base. An analysis is conducted on the change in the modal behaviour of an example two-span piled bridge affected by differently-shaped scour hole development, where scour holes with varying depths and widths are modelled.

The study focuses on how the modal properties of the bridge, specifically the modal periods and mode shapes, vary in both the traffic and

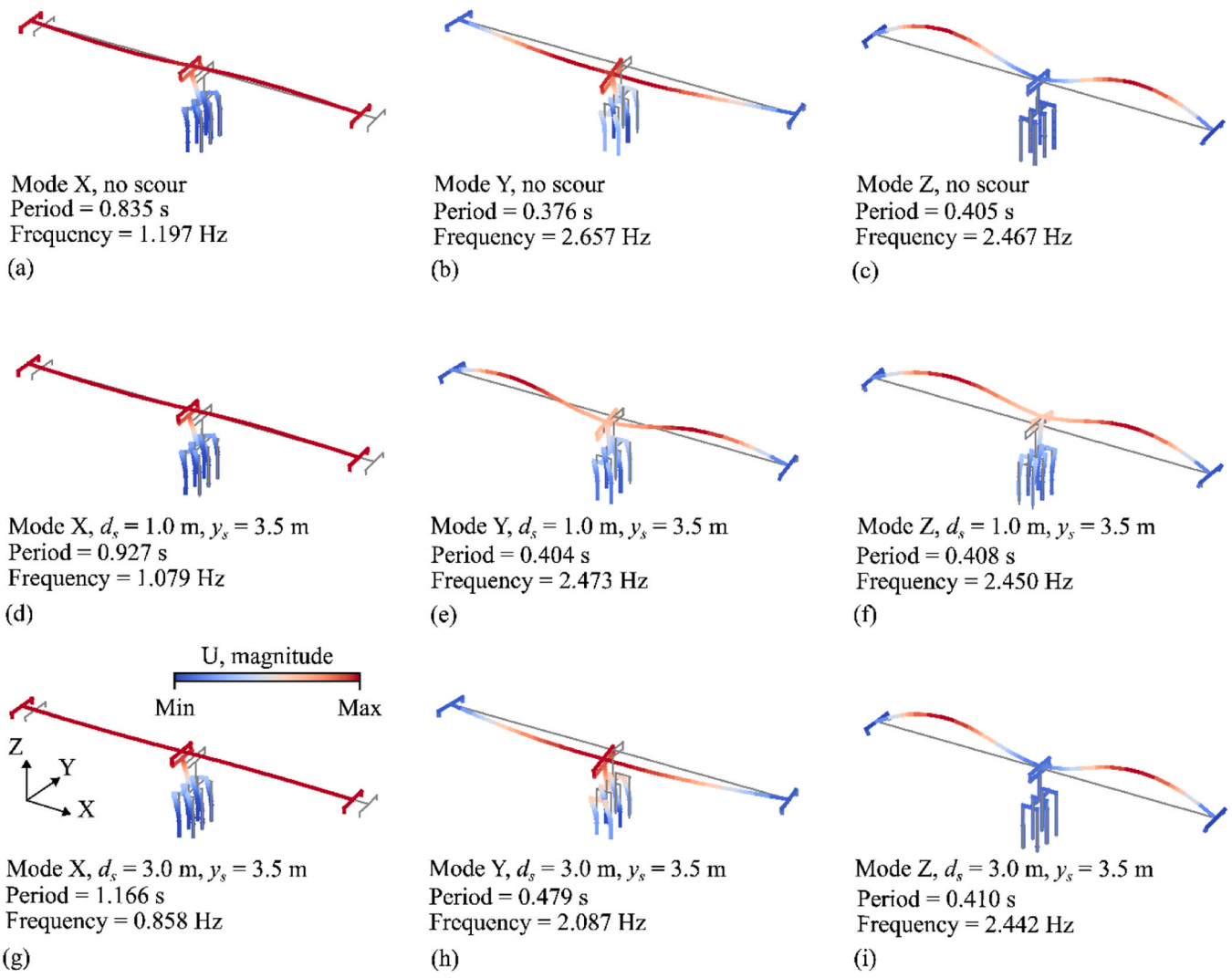

Fig. 12. Global mode shapes of the unscoured bridge and the corresponding mode shapes of the bridge under two scour scenarios in (a, d, g) traffic, (b, e, h) flow, and (c, f, i) vertical direction – medium dense soil profile.

flow directions as scour hole depth and width increase. Three different foundations and soil densities are considered, corresponding to loose, medium-dense, and dense sand profiles, with the pile properties varied to provide the same FoS against axial capacity failure for the purpose of comparison. Modal periods and mode shapes before and after scour are compared, with mode shapes benchmarked using MAC values. In general, a smooth increase in modal periods is observed as scour depth and width increase for a given soil profile. For the medium dense profile and the considered bridge, this is observed to be less smooth. An analysis of the change in MAC values between scoured and unscoured conditions reveals that mode coupling can occur for a certain soil density, scour depth, and width, which gives an apparent decrease in the MAC value under certain conditions. This results from the mode shapes in different directions, such as in the flow direction and vertical direction, becoming coupled due to the aligning of the modal periods. This has practical implications for asset managers implementing vibration-based structural health monitoring approaches on scour-affected bridges, as it can mask the true scour condition if the modal behaviour is not well-understood. It should be noted that water-added mass effects are not considered, as the presence of water is not explicitly modelled. This would have the effect of increasing the absolute values of the modal periods, but no influence on the observed trends are expected.

The main contribution of the work is a practical method to modify soil springs to account for scour hole shapes (varying depth, width, and slope angle), facilitating practitioners to understand the likely changes in behaviour that can result from scour development. The findings of the case study conducted are relevant to the field of vibration-based structural health monitoring of bridges affected by scour erosion. Specifically, the results suggest that data-driven health monitoring may be impacted by unforeseen modal coupling under certain damage conditions, and highlights the importance of model-based methods that can shed light on the physics underlying observed phenomena. Without the capability to practically model scour hole shape influences in physics-based bridge models, this behaviour would be difficult to predict. An example real-world application of the model lies in the development of digital twins of scour-affected bridges, used for the purpose of benchmarking SHM data from a real structure against likely scour conditions affecting a target structure. By varying scour hole shape parameters in the reference (digital twin) model, practitioners would be able to assess the sensitivity of the real structure to variations in scour hole dimensions, and moreover understand if mode coupling or other effects might pose issues to the infrastructure. The practical nature of the model and the ease of use with Winkler-based SSI models is a tangible benefit to the method. The results of this study are therefore likely to interest asset management agencies and practitioners implementing vibration-based bridge scour monitoring.

The developed model can be enhanced with a number of considerations. In the present paper, three foundation schemes providing a FOS

against axial capacity failure of 2 were considered. Future studies should explore different FOS values and how they influence the results. Moreover, the derivation of the effective stress to account for the overburden assumes plain strain conditions and a 2D area ratio. In order to consider non-uniform scour conditions, the approach would need to consider the 3D volume of the scour hole. Additionally, the method has only been developed for unform sand sites. Multi-layered or clay sites requires further model development. These enhancements to the method should be conducted as part of future work. The method has been developed in the present work for application to bridges. It can equally be modified and applied in other contexts such as offshore wind turbine foundation scour monitoring. Finally, the method should be trialled against experimental measurements of the modal responses of real piled bridges affected by scour with varying dimensions, to ascertain the accuracy of the framework. This is required before firm conclusions on the performance and sensitivity of the method can be provided.

CRediT authorship contribution statement

M. Kosič: Conceptualization, Data curation, Formal analysis, Funding acquisition, Investigation, Methodology, Software, Writing – original draft, Writing – review & editing. **L.J. Prendergast:** Conceptualization, Formal analysis, Funding acquisition, Investigation, Methodology, Software, Writing – original draft, Writing – review & editing. **A. Anžlin:** Conceptualization, Project administration, Formal analysis, Funding acquisition, Investigation, Methodology, Software, Writing – original draft, Writing – review & editing.

Declaration of Competing Interest

The authors declare that they have no known competing financial interests or personal relationships that could have appeared to influence the work reported in this paper.

Acknowledgements

The authors would like to express their gratitude for the support received from the Slovenian Research Agency research core funding No. P2–0273 and infrastructure programme No. I0–0032. Part of this research was also funded by European Union Civil Protection Mechanism, under UCPM-2019-PP-AG call, Grant Agreement Number 874421, oVERFLOw project (Vulnerability assessment of embankments and bridges exposed to flooding hazard). The second author wishes to thank Slovenian National Building and Civil Engineering Institute and University of Nottingham for travel funding to facilitate this collaboration.

APPENDIX A

Table A.1
Properties of bridge elements used in the numerical model

Element	E (kN/m^2)	G (kN/m^2)	γ (kN/m^3)	A (m^2)	I_{xx} (m^4)	I_{yy} (m^4)	I_{zz} (m^4)	A_{sy} (m^2)	A_{sz} (m^2)
Deck 1	2.1E+ 08	8.1E+ 07	77	0.41	0.0035	0.1694	6.64	0.041	0.036
Deck 2	2.1E+ 08	8.1E+ 07	77	0.45	0.0035	0.2435	7.74	0.042	0.037
Deck 3	2.1E+ 08	8.1E+ 07	77	0.49	0.0036	0.3188	8.83	0.042	0.038
Deck 4	2.1E+ 08	8.1E+ 07	77	0.53	0.0038	0.3963	9.90	0.042	0.039
Deck 5	2.1E+ 08	8.1E+ 07	77	0.61	0.0045	0.5580	12.06	0.042	0.040
Deck 6	2.1E+ 08	8.1E+ 07	77	0.65	0.0050	0.6424	13.14	0.043	0.041
Deck 7	2.1E+ 08	8.1E+ 07	77	0.69	0.0056	0.7293	14.21	0.043	0.042
Pier	3.1E+ 07	1.3E+ 07	25	22.51	22.30	5.90	294.22	18.91	19.08
Stiff	2.1E+ 14	8.1E+ 13	0	0.25	0.0088	0.0052	0.01	0.208	0.208

APPENDIX B. – Summary of results obtained for dense soil profile

This appendix provides a summary of results related to the impact of scour on global vibration periods and mode shapes for the case of the dense soil profile. Fig. B1 presents the relative change of the global vibration period in both directions for different scour conditions affecting the bridge with a dense soil profile. The results show trends similar to those obtained for the medium dense soil profile in Fig. 9, namely a smooth increase in vibration period with increasing d_s and y_s in the longitudinal (traffic) direction in Fig. B1(a), and mode coupling between the global transverse and vertical modes resulting in a non-smooth increase in vibration period at particular scour conditions in the flow direction in Fig. B1(b). In the longitudinal (traffic) direction in Fig. B1(a), for scour depths exceeding 4.5 m, a significant shift in modal periods is observed, which is a function of the extreme scour-related stiffness loss in the foundation, resulting in rigid body behaviour and a likely exceedance of capacity (not modelled).

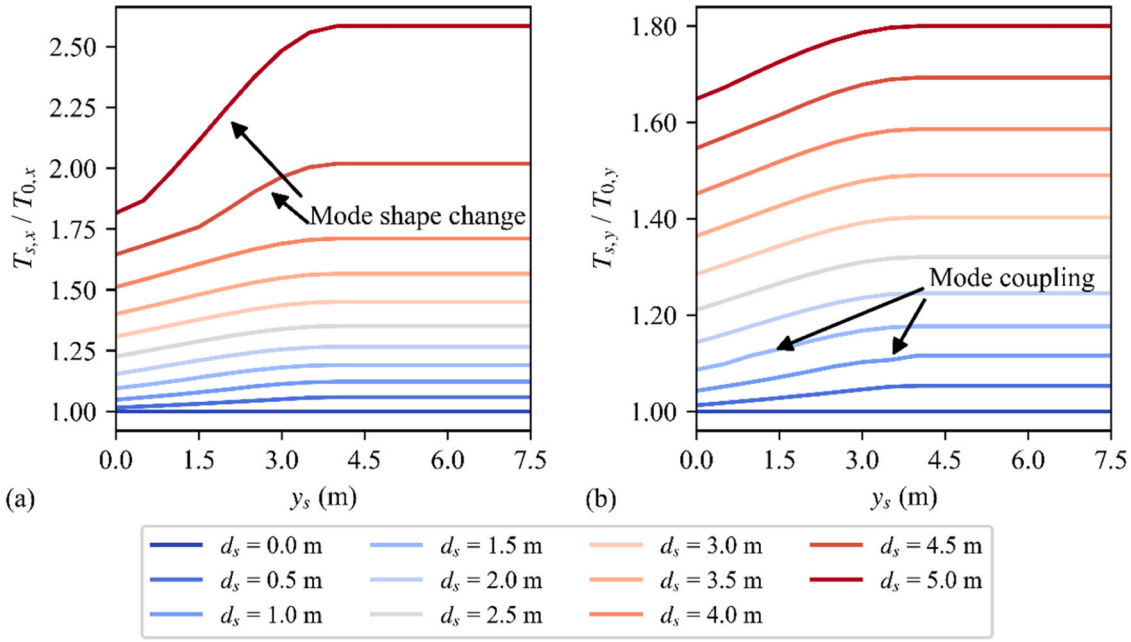

Fig. B1. Relative change of global vibration period in (a) traffic, and (b) flow direction for different scour depths (d_s) and widths (y_s) – dense soil profile

The effects observed in Fig. B1 are also visible in the MAC plots presented in Fig. B2, which show the change in MAC values between the unscoured bridge modes and the scoured bridge modes for various scour conditions in the traffic and flow directions for dense soil conditions. In general, scour leads to a gradual decrease in MAC values as the boundary conditions of the bridge progressively deviate from the initial, unscoured state. However, when mode coupling occurs, a pronounced drop in MAC values is observed, since the resulting mode shape does not exist in the unscoured bridge. For scour depths exceeding 4.5 m, the change in MAC is more complex as the foundation behaviour changes as a result of the extreme scour altering the mechanism of bending to rigid-body rotation. These data are included for completeness, but it should be noted that in a real structure the bridge would likely have exceeded its capacity for these cases.

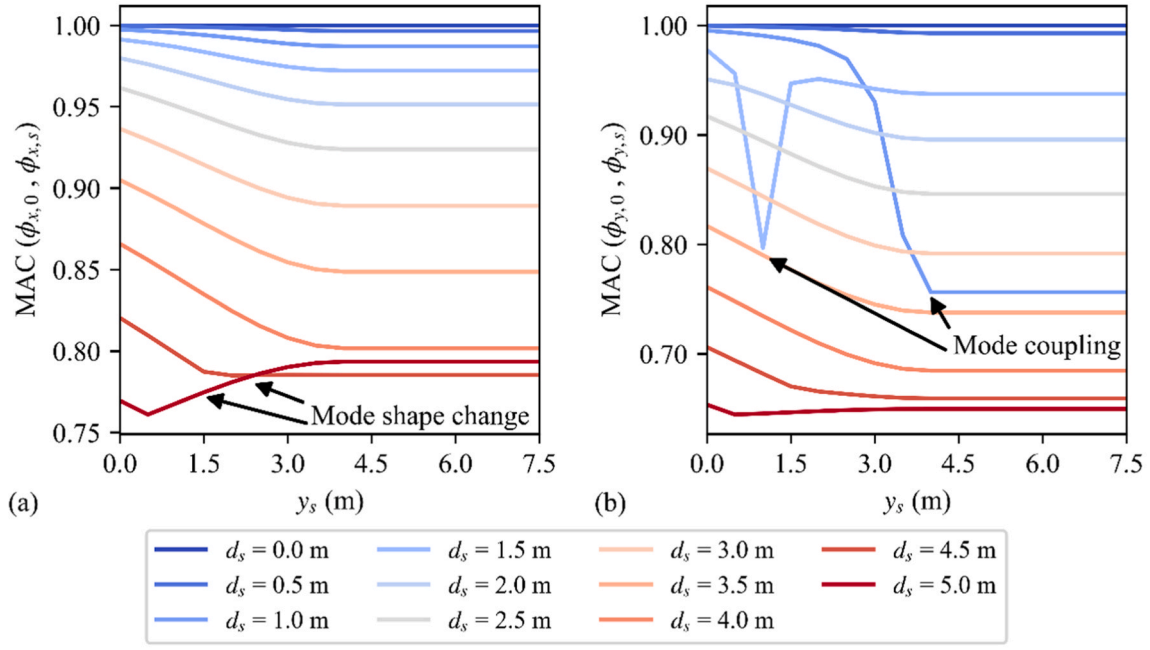

Fig. B2. MAC values of the (a) traffic, and (b) flow direction mode shape under different scour conditions, benchmarked against the mode shape of the unscoured bridge – dense soil profile

References

[1] Intergovernmental Panel on Climate Change (IPCC). Weather and Climate Extreme Events in a Changing Climate. Climate Change 2021 – The Physical Science Basis. Cambridge University Press; 2023. p. 1513–766. https://doi.org/10.1017/9781009157896.013.
[2] Hamill L. Bridge Hydraulics. London: E.& F.N. Spon; 1999.
[3] Prendergast LJ, Gavin K. A review of bridge scour monitoring techniques. J Rock Mech Geotech Eng 2014;6:138–49. https://doi.org/10.1016/j.jrmge.2014.01.007.

[4] Forde MC, McCann DM, Clark MR, Broughton KJ, Fenning PJ, Brown A. Radar measurement of bridge scour. NDTE Int 1999;32:481–92.
[5] Federico F, Silvagni G, Volpi F. Scour vulnerability of river bridge piers. J Geotech Geoenviron Eng 2003;129:890–900.
[6] Heidarpour M, Afzalimehr H, Izadinia E. Reduction of local scour around bridge pier groups using collars. Int J Sediment Res 2010;25:411–22. https://doi.org/10.1016/S1001-6279(11)60008-5.
[7] Barrie A, Wang C, Liang F, Qi W. Experimental investigation on the mechanism of local scour around a cylindrical coastal pile foundation considering sloping bed conditions. Ocean Eng 2024;312. https://doi.org/10.1016/j.oceaneng.2024.119225.
[8] Melville BW, Coleman SE. Bridge scour. Highlands Ranch, CO: Water Resources Publications; 2000.
[9] Wang C, Yu X, Liang F. A review of bridge scour: mechanism, estimation, monitoring and countermeasures. Nat Hazards 2017;87:1881–906. https://doi.org/10.1007/s11069-017-2842-2.
[10] May R.W.P., Ackers J.C., Kirby A.M. Manual on scour at bridges and other hydraulic structures. London: 2002.
[11] Kosič M, Prendergast LJ, Anžlin A. Analysis of the response of a roadway bridge under extreme flooding-related events: Scour and debris-loading. Eng Struct 2023;279. https://doi.org/10.1016/j.engstruct.2023.115607.
[12] Wang C, Wu Q, Liang J, Liang F, Yu X (Bill). Establishment and implementation of an artificial intelligent flume for investigating local scour around underwater foundations. Transp Geotech 2024;49. https://doi.org/10.1016/j.trgeo.2024.101433.
[13] Prendergast LJ, Limongelli MP, Ademovic N, Anzlin A, Gavin KG, Zanini MA. Structural Health Monitoring for Performance Assessment of Bridges under Flooding and Seismic Actions. Struct Eng Int 2018;28:296–307.
[14] Wardhana K, Hadipriono FC. Analysis of Recent Bridge Failures in the United States. J Perform Constr Facil 2003;17:144–51. https://doi.org/10.1061/(ASCE)0887-3828(2003)17:3(144).
[15] Hunt B.E. NCHRP synthesis 396: Monitoring Scour Critical Bridges - A Synthesis of Highway Practice. Washington, DC: 2009.
[16] Briaud J.L., Hurlebaus S., Chang K., Yao C., Sharma H., Yu O., et al. Realtime monitoring of bridge scour using remote monitoring technology. vol. 7. Austin, TX: 2011.
[17] Yu X. Time Domain Reflectometry Automatic Bridge Scour Measurement System: Principles and Potentials. Struct Health Monit 2009;8:463–76. https://doi.org/10.1177/1475921709340965.
[18] Fisher M, Chowdhury MdN, Khan A a, Atamturktur S. An evaluation of scour measurement devices. Flow Meas Instrum 2013;33:55–67. https://doi.org/10.1016/j.flowmeasinst.2013.05.001.
[19] Nassif H., Ertekin A.O., Davis J. Evaluation of Bridge Scour Monitoring Methods. Trenton, NJ: 2002.
[20] Anderson NL, Ismael AM, Thitimakorn T. Ground-Penetrating Radar: A Tool for Monitoring Bridge Scour. Environ Eng Geosci 2007;XIII:1–10.
[21] Zarafshan A, Iranmanesh A, Ansari F. Vibration-Based Method and Sensor for Monitoring of Bridge Scour. J Bridge Eng 2012;17:829–38. https://doi.org/10.1061/(ASCE)BE.1943-5592.0000362.
[22] De Falco F, Mele R. The monitoring of bridges for scour by sonar and sedimetri. NDTE Int 2002;35:117–23.
[23] González A, Hester D. An investigation into the acceleration response of a damaged beam-type structure to a moving force. J Sound Vib 2013;332:3201–17. https://doi.org/10.1016/j.jsv.2013.01.024.
[24] Hester D, González A. A wavelet-based damage detection algorithm based on bridge acceleration response to a vehicle. Mech Syst Signal Process 2012;28:145–66. https://doi.org/10.1016/j.ymssp.2011.06.007.
[25] Law SS, Zhu XQ. Dynamic behavior of damaged concrete bridge structures under moving vehicular loads. Eng Struct 2004;26:1279–93. https://doi.org/10.1016/j.engstruct.2004.04.007.
[26] Cacciola P, Impollonia N, Muscolino G. Crack detection and location in a damaged beam vibrating under white noise. Comput Struct 2003;81:1773–82. https://doi.org/10.1016/S0045-7949(03)00201-3.
[27] Gentile A, Messina A. On the continuous wavelet transforms applied to discrete vibrational data for detecting open cracks in damaged beams. Int J Solids Struct 2003;40:295–315. https://doi.org/10.1016/S0020-7683(02)00548-6.
[28] Doebling S., Farrar C., Prime M.B., Shevitz D.W. Damage identification and health monitoring of structural and mechanical systems from changes in their vibration characteristics: a literature review. Los Alamos, New Mexico: 1996.
[29] Prendergast LJ, Hester D, Gavin K, O'Sullivan JJ. An investigation of the changes in the natural frequency of a pile affected by scour. J Sound Vib 2013;332:6685–702. https://doi.org/10.1016/j.jsv.2013.08.020i.
[30] Prendergast LJ, Gavin K. A comparison of initial stiffness formulations for small-strain soil – pile dynamic Winkler modelling. Soil Dyn Earthq Eng 2016;81:27–41. https://doi.org/10.1016/j.soildyn.2015.11.006.
[31] Winkler E. Theory of elasticity and strength. Dominicus Prague: 1867.
[32] Prendergast LJ, Hester D, Gavin K. Determining the presence of scour around bridge foundations using vehicle-induced vibrations. J Bridge Eng 2016;21. https://doi.org/10.1061/(ASCE)BE.1943-5592.0000931.
[33] Prendergast LJ, Gavin K, Hester D. Isolating the location of scour-induced stiffness loss in bridges using local modal behaviour. J Civ Struct Health Monit 2017;7:483–503. https://doi.org/10.1007/s13349-017-0238-3.
[34] Prendergast LJ, Hester D, Gavin K. Development of a Vehicle-Bridge-Soil Dynamic Interaction Model for Scour Damage Modelling. Shock Vib 2016;2016. https://doi.org/10.1155/2016/7871089.
[35] Kong X, Cai CS. Scour Effect on Bridge and Vehicle Responses under Bridge-Vehicle-Wave Interaction. J Bridge Eng 2016;21:1–16. https://doi.org/10.1061/(ASCE)BE.1943-5592.0000868.
[36] Chen C-C, Wu W-H, Shih F, Wang S-W. Scour evaluation for foundation of a cable-stayed bridge based on ambient vibration measurements of superstructure. NDT E Int 2014;66:16–27. https://doi.org/10.1016/j.ndteint.2014.04.005.
[37] Ju SH. Determination of scoured bridge natural frequencies with soil–structure interaction. Soil Dyn Earthq Eng 2013;55:247–54. https://doi.org/10.1016/j.soildyn.2013.09.015.
[38] Malekjafarian A, Kim C, Obrien EJ, Prendergast LJ, Fitzgerald PC, Nakajima S. Experimental demonstration of a mode shape-based scour monitoring method for multi-span bridges with shallow foundations. J Bridge Eng 2020;25. https://doi.org/10.1061/(ASCE)BE.1943-5592.0001586.
[39] Malekjafarian A, Prendergast LJ, OBrien EJ. Use of mode shape ratios for pier scour monitoring in two-span integral bridges under changing environmental conditions. Can J Civ Eng 2020;47:962–73. https://doi.org/10.1139/cjce-2018-0800.
[40] Khan MA, McCrum DP, Prendergast LJ, OBrien EJ, Fitzgerald PC, Kim C-W. Laboratory investigation of a bridge scour monitoring method using decentralized modal analysis. Struct Health Monit 2021. https://doi.org/10.1177/1475921720985122.
[41] Li S, He S, Li H, Jin Y. Scour Depth Determination of Bridge Piers Based on Time-Varying Modal Parameters: Application to Hangzhou Bay Bridge. J Bridge Eng 2017;22. https://doi.org/10.1061/(ASCE)BE.1943-5592.0001154.
[42] Xiong W, Kong B, Tang P, Ye J. Vibration-Based Identification for the Presence of Scouring of Cable-Stayed Bridges. J Aerosp Eng 2018;31. https://doi.org/10.1061/(ASCE)AS.1943-5525.0000826.
[43] Elsaid A, Seracino R. Rapid assessment of foundation scour using the dynamic features of bridge superstructure. Constr Build Mater 2014;50:42–9. https://doi.org/10.1016/j.conbuildmat.2013.08.079.
[44] Fitzgerald PC, Malekjafarian A, Cantero D, OBrien EJ, Prendergast LJ. Drive-by scour monitoring of railway bridges using a wavelet-based approach. Eng Struct 2019;191:1–11. https://doi.org/10.1016/j.engstruct.2019.04.046.
[45] McGeown C, Hester D, OBrien EJ, Kim CW, Fitzgerald P, Pakrashi V. Condition Monitoring of Railway Bridges Using Vehicle Pitch to Detect Scour. Sensors 2024;24. https://doi.org/10.3390/s24051684.
[46] Bao T, Andrew Swartz R, Vitton S, Sun Y, Zhang C, Liu Z. Critical insights for advanced bridge scour detection using the natural frequency. J Sound Vib 2017;386:116–33. https://doi.org/10.1016/j.jsv.2016.06.039.
[47] Lin C, Bennett C, Han J, Parsons RL. Scour effects on the response of laterally loaded piles considering stress history of sand. Comput Geotech 2010;37:1008–14.
[48] Zhang H, Chen S, Liang F. Effects of scour-hole dimensions and soil stress history on the behavior of laterally loaded piles in soft clay under scour conditions. Comput Geotech 2017;84:198–209. https://doi.org/10.1016/j.compgeo.2016.12.008.
[49] Lin C, Han J, Bennett C, Parsons RL. Analysis of Laterally Loaded Piles in Sand Considering Scour Hole Dimensions. J Geotech Geoenviron Eng 2014;140:1–13. https://doi.org/10.1061/(asce)gt.1943-5606.0001111.
[50] Lin C, Han J, Bennett C, Parsons RL. Analysis of laterally loaded piles in soft clay considering scour-hole dimensions. Ocean Eng 2016;111:461–70. https://doi.org/10.1016/j.oceaneng.2015.11.029.
[51] Wu Q, Wang C, Zhang H, Wang Y, Wang J, Liang F. Numerical investigation on the lateral behavior of scour-affected tripod foundation for offshore wind turbine with solidified soil remediation. Ocean Eng 2025;326. https://doi.org/10.1016/j.oceaneng.2025.120864.
[52] Prendergast LJ, Gavin K, Doherty P. An investigation into the effect of scour on the natural frequency of an offshore wind turbine. Ocean Eng 2015;101:1–11. https://doi.org/10.1016/j.oceaneng.2015.04.017.
[53] Jawalageri S, Prendergast LJ, Jalilvand S, Malekjafarian A. Effect of scour erosion on mode shapes of a 5 MW monopile-supported offshore wind turbine. Ocean Eng 2022;266. https://doi.org/10.1016/j.oceaneng.2022.113131.
[54] Prendergast LJ, Reale C, Gavin K. Probabilistic examination of the change in eigenfrequencies of an offshore wind turbine under progressive scour incorporating soil spatial variability. Mar Struct 2018;57:87–104. https://doi.org/10.1016/j.marstruc.2017.09.009.
[55] Peder Hyldal Sørensen S, Bo Ibsen L. Assessment of foundation design for offshore monopiles unprotected against scour. Ocean Eng 2013;63:17–25. https://doi.org/10.1016/j.oceaneng.2013.01.016.
[56] Ma H, Chen C. Scour protection assessment of monopile foundation design for offshore wind turbines. Ocean Eng 2021;231:1–14. https://doi.org/10.1016/j.oceaneng.2021.109083.
[57] Jiang W, Ph D, Lin C, Ph D. Lateral responses of monopile-supported offshore wind turbines in sands under combined effects of scour and earthquakes. Soil Dyn Earthq Eng 2022;155:107193. https://doi.org/10.1016/j.soildyn.2022.107193.
[58] Menéndez-Vicente C, López-Querol S, Bhattacharya S, Simons R. Numerical study on the effects of scour on monopile foundations for Offshore Wind Turbines: The case of Robin Rigg wind farm. Soil Dyn Earthq Eng 2023;167. https://doi.org/10.1016/j.soildyn.2023.107803.
[59] Tubaldi E, Antonopoulos C, Mitoulis SA, Argyroudis S, Gara F, Ragni L, et al. Field tests and numerical analysis of the effects of scour on a full-scale soil–foundation–structural system. J Civ Struct Health Monit 2023;13:1461–81. https://doi.org/10.1007/s13349-022-00608-x.
[60] Li Q, Prendergast LJ, Askarinejad A, Chortis G, Gavin K. Centrifuge modeling of the impact of local and global scour erosion on the monotonic lateral response of a monopile in sand. Geotech Test J 2020;43. https://doi.org/10.1520/GTJ20180322.

[61] Chortis G, Askarinejad A, Prendergast LJ, Li Q, Gavin K. Influence of scour depth and type on p–y curves for monopiles in sand under monotonic lateral loading in a geotechnical centrifuge. Ocean Eng 2020;197:106838. https://doi.org/10.1016/j.oceaneng.2019.106838.
[62] Meyerhof GG. Bearing capacity and settlement of pile foundations. J Geotech Eng Div ASCE 1976;102:195–228.
[63] Zhu M. The OpenSeesPy Library, Version 3.2.2 – 2020. 2020.
[64] McKenna F. OpenSees: A Framework for Earthquake Engineering Simulation. Comput Sci Eng 2011;13:58–66. https://doi.org/10.1109/MCSE.2011.66.
[65] Kwon YW, Bang H. The Finite Element Method using MATLAB. Boca Raton, FL: CRC Press, Inc; 2000.
[66] OpenSeesWiki - PySimple 1 Material. n.d. ⟨https://opensees.berkeley.edu/wiki/index.php/PySimple1_Material⟩.
[67] OpenSeesWiki - TzSimple1 Material n.d. ⟨https://opensees.berkeley.edu/wiki/index.php/TzSimple1_Material⟩.
[68] OpenSeesWiki - QzSimple 1 Material n.d. ⟨https://opensees.berkeley.edu/wiki/index.php/QzSimple1_Material⟩.
[69] API. Recommended Practice for Planning, Designing and Constructing Fixed Offshore Platforms—Working Stress Design. Washington, D.C.: 2003.
[70] Reese LC, Van Impe WF. Single Piles and Pile Groups Under Lateral Loading. second ed. CRC Press, Taylor & Francis Group; 2011.
[71] Mosher R. Load-transfer Criteria for Numerical Analysis of Axially Loaded Piles in Sand. Final Report Army Engineer Waterways Experiment Station, Vicksburg, Mississippi: 1984.
[72] American Petroleum Institute. Recommended Practice for Planning, Designing and Constructing Fixed Offshore Platforms — Working Stress Design. Api Recommended Practice 2007;24-WSD:242.
[73] Vijayvergiya VN. Load-movement characteristics of piles. 4th Annual Symposium of the Waterway. Port, Coastal, and Ocean Division, Los Angeles, US: ASCE; 1977. p. 1256–66.
[74] Prakasha K., Joer H., Randolph M. Establishing a model testing capability for deep water foundation systems. Proceedings of the 15th International Offshore and Polar Engineering Conference and Exhibition, Seoul, Korea: 2005, p. 309–315.
[75] Clough RW, Penzien J. Dyn Struct 1993.